N/RHD.

UAH8-36955 FR11/1

Final Report

submitted to

NATIONAL AERONAUTICS AND SPACE ADMINISTRATION
GEORGE C. MARSHALL SPACE FLIGHT CENTER, ALABAMA 35812

November 19, 1991

for Contract NAS8 - 36955

Delivery Order 93

entitled

Process Modeling KC-135 Aircraft

by

Gary L. Workman Ph.D.
Principal Investigator

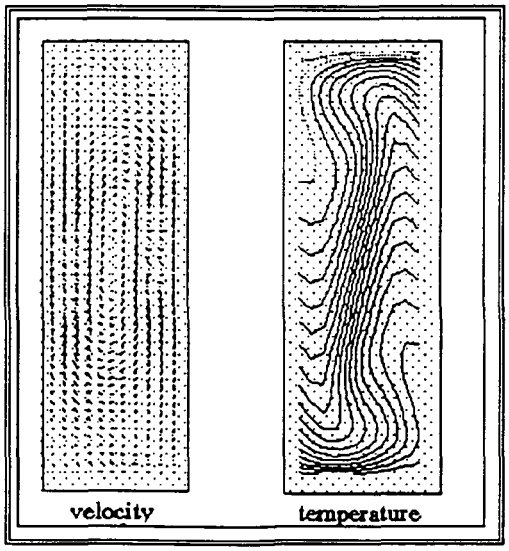

Materials Processing Laboratory
Center for Automation & Robotics
University of Alabama in Huntsville
Huntsville, Alabama 35899

NASA National Aeronautics and Space Administration

Report Documentation Page

1. Report No.	2. Government Accession No.	3. Recipient's Catalog No.

4. Title and Subtitle

Process Modeling for KC-135 Aircraft

5. Report Date

6. Performing Organization Code

7. Author(s)

Gary L. Workman

8. Performing Organization Report No.

10. Work Unit No.

9. Performing Organization Name and Address

University of Alabama in Huntsville
Research Institute, Box 212
Huntsville, Alabama 35899

11. Contract or Grant No.

NAS8-36955

13. Type of Report and Period Covered

Monthly

12. Sponsoring Agency Name and Address

UAH/JRC

14. Sponsoring Agency Code

NASA/MSFC

15. Supplementary Notes

16. Abstract

This program will provide instrumentation for KC-135 aircraft which will provide a quantititative measure of g-level variation during parabolic flights and its effect on experiments which demonstrate differences in results obtained with differences in convective flow. The flight apparatus will provide video recording of the effects of the g-level variations on varying fluid samples. The apparatus will be constructed to be available to fly on the KC-135 during most missions.

17. Key Words (Suggested by Author(s))	18. Distribution Statement

19. Security Classif. (of this report)	20. Security Classif. (of this page)	21. No. of pages	22. Price

TABLE OF CONTENTS

1.0 INTRODUCTION

Many of the space experiments of interest to the commercial and scientific communities are designed to benefit from the microgravity environment found at the altitudes in which the Shuttle currently flies and in which the Space Station will orbit. The major effect of a microgravity environment is its impact on how fluids behave; in particular, the differences which can change process parameters from the normal 1 g process parameters experienced on Earth. Any process involving fluids will behave differently in microgravity. Of particular interest to many scientists is the effect of gravity on materials processing phenomena. Most materials processing experiments involve non-isothermal conditions in liquids, such as crystal growth. A number of fluid parameters are associated with a gravity effect, particularly when density and temperature vary throughout the volume of the experimental sample.

Another option to the microgravity environment of space can considered for feasibility experiments. The 'weightless' environment experienced by occupants of the KC- 135 when the aircraft flies parabolic maneuvers provides a unique testbed for a variety of experiments. The range of experiments which utilize the induced gravity includes physiological, scientific and engineering experiments. The most publicized work has been the many significant results that have been obtained by physiological studies on the effects of reduced gravity on humans and other animals. The KC-135 testbed can also be used for determining human factors requirements in preparing for space flight activities, particularly in practicing for the human's ability to perform particular tasks in microgravity. In preparation for space flight activities, the KC- 135 has provided extraordinary service and cost-savings for pre-space flight validation of procedures and personnel.

In addition to the simulated low gravity experiments on the human element, a number of useful experiments can be performed to check out equipment and physical concepts prior to initiating the huge expense associated with a manifested space flight. Within this concept are a number of materials processing experiments which allows a preliminary look at the effect of reduced gravity on fluid phenomena and solidification experiments. The materials processing community can and has taken advantage of the KC- 135 as such a testbed quite frequently over the years.

Much can be learned about the role of reduced gravity in both the physical activity associated with carrying out a scientific expenment in an environment that is decidedly quite different from the normal laboratory environment and in the physical phenomena being studied in a materials processing expenment. The impact of electrical power and physical constraints of the aircraft itself and the physiological effects on the personnel performing experiments in the varying gravity levels of the aircraft all effect how well an experiment works on the KC-135. The ultimate goal is usually to provide a simulated microgravity environment which allows one to predict how well the same experiment would operate in microgravity and in some fashion extrapolate from the 0.01 g experienced in the KC-135 to 0.00001 g experienced in space. Hence, the quality of the

low gravity period does certainly affect the experimental results obtained and how it should be interpreted.

Low-gravity conditions of the KC-135 are used to control the convective consequences of these non-isothermal processes for short periods of time (20-30 seconds). Too many investigators consider the brief period of low-gravity as 'zero' gravity and ignore the significant accelerations their specimens see in various directions. They also ignore the possibility that fluid flow is not instantly stopped when the aircraft is in low-g and then resumes as quickly in pullout. Veteran users of the KC-135 know that there is significant variation fom parabola to parabola in the quality of the low-g, as well as between pilots and atmospheric conditions. KC-135 experiment packages are rarely free-floaters and are becoming increasingly heavy, necessitating the rigid mounting to the aircraft. Location and placement within the aicraft are also known to have influence over the accelerations 'felt' by an experiment.

The Convective Flow Analyzer (CFA) or Flow Visualization Expenment is a measuring and monitoring device specifically designed to quantify the effects on fluid motion (convection) by the various accelerations generated by Keplerian trajectories on the NASA KC-135 aircraft. A variety of experiments in microgravity materials processing have been performed using the KC-135 as a testbed. None of the experiments have identified nor quantified the exact types of influences on fluid convection during low-gravity maneuvers or parabolas. It is the purpose of the CFA to measure the effects of changes in the acceleration (of gavity) in two directions simultaneously upon convective flow established in a thermal gradient.

1.1 THEORETICAL CONCEPTS

The theoretical development of convective flow and its dependence on g levels has been presented by several authors. For our discussion here we shall present the basic equations to show the dependence of convective flow and the resultant temperature fields on gravity. More enlightning data fiom EASYFLOW calculations are also shown as results from the modeling experiments.

Fluid parameters which affect fluid behavior are usually expressed as dimensionless quantities in order to simplify discussion and make easy comparisons with respect to predicting fluid behavior. Table 1 on the following page includes the materials properties which are of interest to us in order to study free convection phenomena.

Table 1. Material properties of interest to fluid behavior and their normal symbolic representations.

Symbol	Property	Units
a	Thermal Diffusivity	watts / m °K
β_T	Thermal Coefficient of Expansion	°K
c_0	Specific Heat	joules / kg °K
λ	Thermal Conductivity	watts / m °K
ρ	Density	Kg / m^3
ν	Kinematic Viscosity	m^2 /sec

As mentioned in the introduction, fluid behavior which is of interest to this set of experiments are those which are affected by temperature gradients, density differences, and the combination of these physical attributes. The dimensionless parameters which deal directly with these relationships are the Prandtl Number, Grashof Number and Rayleigh Number. Table 2. below defines these quantities.

Table 2. Table defining pertinent relations for fluid flow behavior.

Dimensionless Parameter	Equation
Prandtl Number	$Pr = \frac{\nu}{a}$
Grashof Number	$Gr = \frac{g*\beta_T*L^3*\Delta T}{\nu^2}$
Rayleigh Number	$Ra = Pr*Gr = \frac{g*\beta_T*L^3*\Delta T}{\nu * a}$

The driving forces which affect convective flow are usually formulated in terms of Rayleigh number; however, since the Rayleigh number is defined to be the product of the Prandtl and the Grashof numbers, it is obvious that the physical basis for convective flow can be traced back to these parameters. The Prandtl number determines the relative importance of velocity fields to thermal fields in the material, while the Grashof number determines the ratio of buoyancy forces to viscous forces in the current experimental arrangement. Hence both relationships are included in the makeup of the Raleigh number which is normally used to explain convective flow processes.

2.0 EXPERIMENTAL

A slow-moving convective flow pattern is established in the vertical glass specimen container (1 x 1 x 1 2 cm) by heating the top end resistively. A thermal gradient is established by fixing the temperature of the bottom end of the specimen with a cooling block of brass which is thermoelectricaly cooled. Dispersed within the water (the fluid) are marker (or tracer) particles which follow the local flow vector. The tracer particles used were either latex styrene spheres of 38 micron diameter, or guanine flakes. A high resolution black and white CCD video camera with a macro lens is arranged to view the flow pattern which is illuminated by a thin plane of laser light sent vertically through the specimen normal to the camera axis. Alternatively, the tracers were lighted by top-down illumination of white light passed in to the cell via fiber optic cable. As the tracer particles enter the light beam, they scatter the light into the camera and are recorded. Particle movements within the cell are recorded as tracks which identify local fluid trajectory and velocity. A replicate camera and lens is mounted to view the fluid pattern in a normal axis to the first camea. In this way, aircraft accelerations in all three axes and their combined effects on the fluid patterns are measured. Figure 1 on the next page shows a sketch of the apparatus.

Mounted on the exterior of the cell's wall 5 mm in from the metal hot and cold blocks were small gauge thermocouples. The data acquisition system recorded the temperatures along with the accelerometer data. As will be shown later, thermal fluctuations caused by fluid motion within the cell were observed at these thermocouples.

In the Appendix are the camera resolution calculations for the apparatus configured as employed here. In general, the cell width was displayed on half of a video screen such that the other cell width view would be displayed as the other half video field. Under these circumstances, the camera resolution is practically limited to 45 x 50 micrometers in the vertical and horizontal respectively. This is for tracer particles which are in focus and large enough for the camera to detect. Minimum particle size for this configuration was experimentally determined to be 20 micrometers or more. (Note that resolution is still limited to 45 x 50 micrometers which means that two 20 micrometer particles need to be at least 45 micrometers apart from each other to be seen as two separate particles. Otherwise, the two particles are seen as one.)

Particle velocity measurements are more complex to establish limits of the detectability. Velocity measurements require position and time data. Both pieces of information are readily available from the video playback. Theoretically, the minimum velocity one can measure from the apparatus is 50 micrometers movement in 0.0333 of a second for a frame-to-frame time interval. This amounts to a velocity of 1 .5 x 10^{-3} m/s. Fortunately, we are not requred to measure velocity between frame pairs. If we did, however, this would allow acceleration resolution of 0.045 m/s^2. From model predictions, a lower limit for low gravity flow velocity would be the extremely small value of $5x10^{-6}$ m/s. Given the resolution, and by requiring only a resolution limit of particle travel, this velocity could be detected after 10 seconds of tape playing. This assumes the particle exacty follows the fluid flow. For typical values of gravity (0.01 g vertical and 0.01 g

horizontal) the velocity would be less than 5×10^{-5} m/s. This would require one second of tape play. Depending on which model (those calculated here or other's like Motakev, et al[6,7]) transient damping times for fluid flow in configurations such as those described here, particularly going from unity gravity to 0.01 gravity would range around 4 to 21 seconds. Fluid damping is fluid deceleration from high to low velocities. The apparatus described here cannot measure the deceleration rates for such predicted damping times. To measure the rate of damping, a few velocities would need to be measured between the transient and the fully damped time. Since one velocity measurement (at the limit of the capability of the apparatus) requires typically 1 to 10 seconds, one can only have one velocity which is insufficient for rate determination.

What can be done, however is to measure velocities during a low gravity period (of 15 to 30 seconds duration). Alternatively, rather than measure a velocity, one could watch the tape at an accelerated speed. The human eye can readily detect the particle motions, including the ensemble of particles in the field of view. Particle accelerations or decelerations are markedly discernible (within the resolution of the equipment). Note once again that replay of the video tape at higher speed presents several seconds of particle movement in just one second. Even the human eye has detectability limits. High gravity conditions produced velocities of 1×10^{-3} m/sec, which can be easily measured. The calculated limits described above cannot be taken as the practical or working limits. A variety of effects such as noise, video jitter, and the additive effects of errors in the assumptions made for the calculations collectively limit the detectabilities mentioned to about half as good as the ideal calculations show.

For this apparatus, particle velocity can only be determined for directions normal to the camera lens axis. If a particle were to move at an angle towards or away from the camera, this component of the velocity vector will not be known. If the particle were in focus and seen by the orthogonal camera, this component of velocity could be measured if the particle could be identified (from among the hundreds seen). For the most part, particle motion in the camera field of view was strictly vertical. Convective flows were mostly restricted to circulation in one plane. That is, in an fore-aft, or left-right orientation since the cuvette was aligned with the viewing axis aligned with the aircraft major axis. Occasionally, corner to corner circulation was observed and readily verified by observing both camera views.

Particle motion analysis can be somewhat automated using computer enhanced image analysis techniques. Some of these techniques were tested with the video data taken, A better description of these methods are given later. The princple of analysis is based on the repeated acquisition of digitized frames of the video tape as it plays. The frames are added together as they are collected. Particle positions are displayed as a function of time by forming streaks of light on a dark background. The length of the streak depends on tee particle velocity and the length of time frames were collected. Computer enhancement further clarifies the image and makes velocity measurements simple. For more sensitivity, the frames can be added over a longer time interval. These techniques are now proven to work.

An alternative to computer enhancement was attempted first. This technique used the storage capabilities of photographic film to record the particle position with time as the tape played. The camera's shutter was left open for several seconds (typically 8 seconds) to expose the film to the video monitor' s image. The idea would work but had several limitations due to the lack of tolerance in achieving contrast on the film. The area of the video image represented by particle absence was not a pure black. Instead, due to the lighting, background noise and artificial gray levels set by the video recording process, the particle images which are not pure white but rather a light gray, are washed out by the high image density of the dark background. Dim or small particles may not register. When particle movement was rapid, the exposure could be short and constrast high. However, the method cannot be generally applied.

The cell design was improved to permit adjustment of the position of the bottom of the cell. This adjustment was introduced to observe variations to flow patterns caused by geometry changes of the flow volume. An increase in flow velocity may have been another response to a reduction in aspect ratio. Circulation patterns and their magnitude both are strongly affected by fluid volume dimensions and aspect ratio. For this experiment, adjustment of the aspect ratio was specifically designed to simulate the effect of crystal growth in a Bridgeman-Stockbarger furnace. Some efforts have been made in the past to evaluate convective velocities using analytical models in known, fixed, geometries. No one has addressed the real case where the fluid volume is progressively reduced due to liquid-to-solid transformation dunng crystal growth.

Fluid velocity measurements and flow patterns had to be made from the video taped experiments, where settling of the tracers occured (and it nearly always did), an initial stirring using the included push-rod (or in the earlier model cell, a magnetic stirring bar would distribute the particles and remove the temperature gradient set within the stagnant fluid. From 15 minutes to a half hour of constant recording was preferred. This involved both the video and the data (acceleration) acquisition.

Fluid patterns could be determined by eye from playback of the tapes. The recorder used in this work was capable of playing back the tape at high speed (and slow speed). Since the particle motion was always minimal, fast play of the tape revealed the patterns very well. Velocities could also be gauged, even by the untrained eye, during fast play. Gravity levels, and therefore where transitions from high to low occured, and the elapsed time could be observed from the tape as well. Taken together, it was clear to see how quickly the fluid motions damped upon entering low g segments.

Velocity measurements fom the tapes had to be made by following individual particles through several seconds of tape to obtain the distance traveled per unit time. Motion was so slow that velocity measurements for low g segments required 5 to 8 seconds of tape play to obtain measurable displacements (if there were any). This precluded measuring particle velocities in low g segments with time resolutions small enough to obtain transient responses. However, one can observe directly from the tape that the particle

2.2 ANTICIPATED OBSERVATIONS

Sensitivity of the flow measurement depends upon the flow rates created and the methods of measurement. In this experiment, flow is anticipated to nearly cease when thermal buoyancy is reduced to extremely low levels. Under these circumstances, sensitivity is important for flow velocity to be measured. Sensitivity to flow at small velocities in this experiment requires that the tracking particles selected be as nearly buoyant as possible. The tracer particles also need to be as large as necessary to scatter light sufficiently to be resolved by the CCD cameras. If particles are small enough, they will not settle quickly due to external accelerations even if they are more or less dense than the fluid. Particles of 20 micrometers diameter are approximately the lower size limit for the optics of the CFA. This was determined for the case when the full cell width is viewed, as opposed to a partial view of the cell at higher magnification and therefore resolution. If water is used as the convecting fluid, styrene latex particles are the tracer material of choice. Their density is 1.05 g/cc. If particles such as these are used, calculated Stokes settling rates of cm per hour are seen. Included here are the calculations for styrene particles in water. Since thermal convection is the prime force, changes to water density and viscosity with temperature the required to be known in detail. The particles are spherical and assumed not to change density significantly with temperature.

The forms of flow patterns that may form include simple loops, double loops, toroidal loops, multiple loops, chaotic flow and non-steady state flow or time variant flow. For the quiescent conditions of crystal growth, however, only smooth, laminar, slow flow is expected and observed in the CFA. multiple loops of flow can occur, but were not observed in the cells. Container volume and shape play a role in determuning the patterns and velocities observed. In this series of experiments, container aspect ratio and volume was adjusted to cover a wider range of fluid dynamic conditions.

The accelerations felt by the experiment are multi-axial. Time variations on these movements vary as well from slow lateral drifts to sudden roll movements due to pilot correction. Accelerometers record some of these movements and an investigator of an experiment can (if they desire) relate the acceleration records to specimen features that may be frozen in place or otherwise recorded. Residual accelerations in other than the z or vertical axis can induce flow pattern changes which differ from the anticipated results if the investigator is ignorent of these small acceleations. This would be the case if an investigator assumes low-g means no-g. In the specimen volumes used in these experiments, lateral accelerations account for as much flow as the vertical ones.

While thermal gradients were used here, solutal gradients can account for similar results. If the thermal and solutal gradients are sufficiently small, the lateral accelerations will produce negligible effects.

2.3 OBSERVATIONS:

It was anticipated before the experiments began that the following sequence of events might be observed:

A steady-state flow loop forms circulating in the forward orientation at high-g. After leaving a low-gravity cycle with a small lateral acceleration, the flow loop returns in high-g but with a circulation in the port-starboard orientation.

Such a scenano was not observed to occur. (It could if the accelerations were appropriate.) Instead, from parabola to parabola, the lateral acceleration signature in time was relatively reproducible. This can be seen from the various accelerometer traces included here. If by pilot control, the lateral acceleration signatures were to shift from front to port-starboard, a re-orientation of the major flow loop would be found to occur. Due to the regularity or reproducibility of the accelerations (weather effects not included) flow patterns during parabolas were consistent and reproducible in the overall view.

TABLE 3. SUMMARY OF FLIGHT EXPERIMENTS ON KC-1 35

Flight File Name	Flight Date	System Studied	High Temp	Cold Temp	Run Time min	Comments
1FEB0591	FEB 5	W,S	UNK	UNK	60	not calibrated
1FEB0691	FEB 6	W,S	UNK	UNK	60	no temp calibrated
1FEB0791	FEB 7	W,S	UNK	UNK		not calibrated
1FEB0891	FEB 8	W,S	UNK	UNK		no temp calibration
W3691S2	MAR 6	W,F	45.5	24.8	15	calibrated
W3691S3	MAR 6	W,F	44.92	26.32	15	calibrated
W3791S1	MAR 7	W,F	44.5	27.35		calibrated
W3791S2	MAR 7	W,F	44.92	27.92		calibrated
W3791S2	MAR 7	W,F	45.11	28.51		calibrated
W3791S3	MAR 7	W,F	43.95	27.34		calibrated
W3791S4	MAR 7	W,F	45.11	28.32		calibrated
W3791S5	MAR 7	W,F	48.24	25		
W3891S1	MAR 8	W,S	48.24	25		
W3891S2	MAR 8	W,S	42.96	27.53	15	heat pulse
B4991S1	APR 9	W,S	40	26	5	
B4991S2	APR 9	W,S	38	11	20	parabola 25
R49011S1	APR 10	W,S	38	13	20	parabola 13
R49011S1	APR 10	W,S	37	12	3	turbulent ride
R49011S1	APR 11	W,S	34	13	6	parabola 4
R49011S1	APR 11	W,S	37	17	10	parabola 23
R49011S1	APR 11	W,S	32	17	10	
R49011S1	APR 12	W,S	33	17	5	parabola 4
R49011S1	APR 12	W,S	41	12	15	parabola 21
1C60491	JUN 4	W,S	51	1	15	rod out
2C60491	JUN 4	W,S	52	4	15	rod out
1C60591	JUN 5	W,S	50	0	15	rod out $\frac{2}{3}$

2C60591	JUN 5	W,S	51	3	13	rod out $\frac{1}{2}$
1C60691	JUN 6	W,S	45	8	15	rod out $\frac{2}{3}$, various volumes
1C070991	JUN 6	W,S	58	4	15	various volumes
1C070991	JUL 9	LNS,F	56	2.5	14	
2C070991	JUL 9	LNS,F	58.4	3.3	15	
1C071091	JUL 10	LNS,F	50.9	3.9	13	
2CO71091	JUL 10	W,S	54.8	3.1	15	
1C071191	JUL 11	W,W	41.9	8	14	half volume
2C071191	JUL 11	W,S	41.2	7.2	15	half volume
1CO71291	JUL 12	W,S	27.3	25.9	4	half volume
2CO71291	JUL 12	W,S	27.1	25.9	15	half volume

Legend: W = water, F = flakes, S = speheres, and LNS = lead nitrate solution.

Based on particle motion studies, fluid velocities were always quite low and near the limit of resolution hr the velocity measurements when low-g segments of the parabolas were examined. From measuaments of particle motion in low-g conditions, velocities ranged from 14 to 57 micrometers per second (or 1.4×10^{-7} to 5.7×10^{-7} m/sec). These values represent velocities observed over various intervals after a high-g segment until the next high-g segment. Stirring caused high velocities of up to 2.8 mm per second (or 2.8×10^{-3} cm/sec). Fluid damping quickly reduced the velocities from stirring to near steady state in a matter of seconds.

Moderate particle motion was usually observed during high-g segments when latex spheres were used as markers. The styrene latex spheres were observed to drift in unison with the high acceleration due to simple sedimentation. The guanine flakes did not have this problem and did not measurably drift due to sedimentation during high-g segments (and clearly not drift in low-g segments). Flake sedimentation velocities were known to be immeasurable for this apparatus and therefore gave a more precise measure of fluid motion.

Another significant observation from the video tapes is that aircraft rotational accelerations (pitch, yaw and roll) as well as accelerations in orthogonal axes (up/down, forward and left/right) caused fluid motions. Circulations within the specimen cells were observed in direct response to (in particular) aircraft roll or axial rotations. Occasionally, aircraft pitch was responsible for similar circulations. These aircraft motions accounted for the greatest short term fluid velocities during any portion of a flight, parabolas or not. In all cases, when these motions caused fluid circulation, it was a simple front to back or left to right circulation loop. This is opposed to the possibility that combined pitch and roll would lead to complex fluid circulations or motion from corner to corner. In all observed cases, the rotation induced motions were in pairs with a brief clockwise (or counteclockwise) followed an equal counterclockwise (or clockwise) motion. Since the pilot or autopilot maintains the proper aircraft attitude, any perturbation like the roll is quickly corrected. The fluid response is immediate under these cases. Following the particle positions through a pair of rotations reveals that the fluid comes to rest in

essentially the same position in which it started. A damping time could not be measured but it appears that the fluid reacted more as a solid body than as an undamped fluid.

Occasionally, the auto-pilot causes a small oscillation such that the fluid circulation reverses a couple of times with each cycle being smaller than the last. Roll effects were most ofen observed during transitions from high to low or low to high g. Some rotation effects were caught during low-g and high-g segments.

Three single axis linear accelerometers cannot measure such motions of the aircraft directly. That is not to say that these motions are not affecting the accelerometers, but rather that the linear three axis accelerometers do not measure the rotational accelerations. Discussions with an accelerometer manufacturer revealed rotational accelerations cannot be derived from a three axis accelerometer such as those used for the KC-135 experiments.

The thermocouples could only be mounted on the cell wall not observed optically. As a result, fluid motion may or may not affect the temperature at a thermocouple depending on the direction the cell was mounted in the aircraft. Usually, the thermocouples were on the left (starboard) side of the cell when the observer faces forward in the plane. On one flight, the left cell face was pointed aft in the plane and the observer faced the left (starboard) side of the plane. In the former case, thermal fluctuations were greatest on the hot thermocouple with increases in temperature abruptly developing at the high-g period while temperatures diminished slowly when 10-g periods occurred. The cold thermocouple showed little response. In the later case, thermal effects were found on both hot and cold thermocouples with more variation on the cold. Additionally, the pattern was different in this latter case as well. The degree of variation was smaller in both hot and cold in the latter case. Variations were seen at both the start and end of the 10-g cycles with little change in temperature occurring during the high-g cycle as with the worst case.

With regard to temperatures, it was initially planned that higher temperatures and different fluids be used in the cells. During the experimentation, it was discovered that the tracer particles selected (which represent the most sensitive types available) could not be heated above 65 °C. The water in the cell also would freeze if cooled below 0 °C and this imposed a lower limit. This limited the thermal gradient that could be applied. As observations were made in the early tests, it became clear that higher viscosity fluids would not provide useful information in the apparatus. As it turned out, based on a search for liquids of low viscosity, the lower the viscosity, the lower the boiling point or evaparation tenperature. Interesting candidate fluids would have produced high pressures or had limits to thermal gradients that prevented their use in the present cell design. A much more expensive cuvette design, and an elaborate cooling system would be needed to use even simple fluids like alcohols or fluorinated hydrocarbons. Common alcohols and suitable candidates for the apparatus happen to behave similar to water to justify replacing the water. The problem also remains to find suitable tracer particles. Some tracer particles like the styrene plastic, glass beads, mica flakes, metallized mylar and vermiculite cannot give the high sensitivity found necessary to make the measurements.

The particles are either too dense, too light, too small, too big or simply incompatible with the liquid. If convective flows under destabilizing conditions such as with Benard cells, Couette flow, or Marangoni now occur, these other schemes could work. It was however, the intention of measuring the effects close to real crystal growth conditions and so the most sensitive methods were needed.

Another sensitive method would be to use immiscible fluids like succinonitrile and an alcohol. A dispersion of the one fluid to make tracer particles in the other would work well except for one new problem. Both the density and composition of the tracer particle phase would change as the particle was carried to the cold or hot zone. This would require far too complex a set of calculations to prepare to model the heat transfer and fluid flow problem. The particles would also change size with time and drift under the influence of the thermal gradient itself This drift would have to be differenced out from the flow measurements. Sedimentation problems would be a minimum since the tracer particle can have nearly the same density than the suspending fluid.

Some experiments were performed with lead nitrate in solution with the water to raise the density of the liquid and thus alter the Reynolds number without altering the viscosity behavior. It turned out that in storage, the flake tracers were destroyed by the lead compound. Tests in the lab previously showed the tracers survived 2 days at room temperature. During transit in a hot truck (well above room temperature) for several days, the tracers turned into fine, nearly colloidal particles barely resolved by the cameras.

3.0 MODELING RESULTS

3.1 Introduction :

A variety of computer models were created for this effort. The 2 or 3 dimensional models were created using a 386-PC based computer program called EasyFlow, a derivative from the same company's Phoenics program. The models provide flow velocity, pressure and temperature distributions of the fluid within the container which is modeled. Results are presented in graphical form using multiple colors, vector lengths and shading to present the temperature, flow and pressure solutions point by point within the model.

3.2 Model Verification:

All models produced reasonable numerical results for the cases tested. Model cases were prepaed specifically to test against other published work. Comparisons of flow velocities and flow patterns were made which confirmed the viability of the model techniques used. Checks were made from model to model to confirm consistent results. For example, a 2-D model should yield similar results to a 3-D model for the same initial conditions. Comparisons were also made between the model and the experimental observations.

3.3 Modeling

Models for the CFA work are unique in the fluid modeling fiield since the conditions examined in the CFA are not very dramatic or dynamic. The thermal boundary conditions set for the models are of a stabilizing nature and should theoretically lead to no free convection at all (even with unity gravity acting downwards). Since this is the arrangement of choice for the crystal growers, it is this, more representative scheme that was employed experimentally and modeled. Due to the very small velocities involved, the detail of the models and the low mathematical stability of the model conditions, long periods of time (hours) were needed for the computer model to reach convergence. Each run of a very simple 2-D model would take 10 minutes and convergence would be reached after 100 or more iterations. For proper convergence, some runs for steady state conditions needed 500-600 iterations with run durations of 3 hours or more. EasyFlow has a convergence monitor display mode that permits real-time checking of the calculations during a run.

Convergence of individual parameters are plotted with time on the screen in the convergence monitor mode. One can determine which converge quickly and which converge slowly thus allowing intelligent modification of the model to increase accuracy and speed in subsequent runs. The simpler 2-D models used approximately 10 by 30 grid points where the width and height of the cell were segmented into these elements. This computational fluid dynamics software is not a finite element type, but one can imagine that it is in order to conceptualize these computations.

Modeling can be separated into two categories, steady state and transient. The easiest efforts during this work were to determine the steady-state flows one would obtain in the specimen for a variety of conditions. (Others have made similar calculations among these lines.) Once models were confirmed to be viable in 2-D, and 3-D, then transient modeling was performed. Much of the work was done in 2-D models due to the extreme time usage for 3-D transient modeling, although considerable work was performed in 3-D models as well. The transient models were configured to show how the fluid in the cell would respond when the aircraft parabolic trajectory would cause a snap change in acceleration from approximately 1.8 g vertical to 0.01 g vertical. There is no previous work in the literature such as this.

In addition to flow velocities, temperatures at a point in the cell are also presented (as well as pressures but they not used). Comparisons were made between temperatures during transient modeling snd temperature changes actually measured in the flight measurements.

The important parameters for convective flow are the Raleigh (Ra and Prandtl (Pr) numbers and the cell aspect ratio. For water, with Pr=6.7, G. Muller et al established a stability diagram denoting the relationship between Ra and aspect ratio. The first Easyflow models prepared verified the results of Muller's paper.[1,2]

3.4 Results from Modeling:

3.4.1 Brief Modeling Results.

Essentially two things were learned from the models. One, the models predicted behavior just as well as other attempts at modeling in the past. The models prepared here were far more sophisticated than others in regard to a) treating stable convection, b) using a 3D approach and c) performing transient condictions, The other, was that the models provided independent order of magnitude values for comparison to the experiments. From the models, temperature profiles, fluid velocity magnitudes and vectors, flow patterns and the various transient effects could all be obtained.

One set of results supports or verifies the other. Where fluid velocity measurements did not reveal sensitvity, temperature measurements did. The models provided temperature behavior which was matched to the measured temperature fluctuations on the cells.

3.4.2 Detailed Analysis of Modeling Results

3.4.2.1 Results From Steady State Models

From the results of modeling steady state convection for comparison to Muller et al's [1,2] work , we saw that the onset of convective flow occured at critical Ra number. Furthermore, the larger the Ra number was, the greater the maximum convective flow velocity. One may refer to the following chart. For a given aspect ratio, so long as the Ra number is the same, the maximum flow velocity will also be the same. A result of this is that if the temperature gradient is raised and if the acceleration of gravity is reduced to the same degree, then the maximum flow velocities will be the the same. For all modeling results, velocities will be in units of meters per second (m/s) and are named respectively U,V,W for the x, y and z directions. For all cases, y is up/down, x is left/right and z in in/out.

Steady State Results Chart

For height=68 mm, width=15 mm, aspect ratio=H/W= 4.53;
for top wall being cold, and bottom wall being hot;
with side walls adiabatic (no heat loss or exchange);
with water having Pr= 6.7 and where a = 2.275 10^{-4} and k = 1.415 x 10^{-3} cm^2/s
and ν = 9.63 x 10^{-3} cm^2/s; then:

Case	R_a	Gravity	ΔT	Max velocity (m/s)
1	8 x 10^5	1	0.15	2.11 x 10^{-4}
2	1 x 10^7	1	2	1.02 x 10^{-3}
3	8 x 10^3	0.01	0.15	1.08 x 10-^{10}
4	8 x 10^5	0.01	15	2.11 x 10^{-4}

3 .4.2.2 Results From Transient Models

Transient modeling is the most difficult of all to do. The object is to take snapshots of the fluid behavior as it constantly changes from one state to another when perturbed. If there were no perturbation, the steedy state values would be reported. However, the KC-135 must undergo parabolic trajectories which lead to sudden and large changes in acceleration. The consequences of these accelerations is one main area of interest in these experiments and models. Most interest is focused on the g-level changes from high to low. It was decided to apply two accelerations on the models since reality is never ideal. Vertical acceleration was set to 1 g and horizontal acceleration was set to 0.01 g. From these conditions and the experimental arrangement, a model was run to generate the initial state prior to the tine for the transient. The steady state results from this condition are the baseline for the transient models.

For the first transient model set, a 2-D analysis was performed with three cases. Each case represents a change in g-level in one or both axes, The results are outlined in the following 2-D Transient Chart. Transient effects were modeled for 20 seconds worth of time cut and inspected every second. Thus, the first transient we studied was 1 second fom the assumed onset of the g-level change. Furthermore, to ensure that 20 seconds was a reasonable period, a steady state solution for each transient analysis was evaluated. This represents the conditions in the cell at infnite time after the perturbation.

2-D Transient Results Chart

For height = 68 mm, width=15 mm, aspect ratio=H/W = 4.53;
for top wall hot @ 50 C, and bottom wall cold @ 25 C;
with side walls adiabaic (no heat loss or exchange);
with water having Pr = 6.7 and where $a=3.619 \times 10^{-4}$ and
$k = 1.494 \times 10^{-3}$ cm/s and $V = 6.902 \times 10^{-3}$ cm^2/s; with $\Delta T=25^\circ$ and starting conditions of steady state 1g in Y and 0.0l g in X where $u=2.78 \times 10^{-9}$ and $V=8.93 \times 10^{-8}$;
then:

CASE	Gravity	Max Velocity	Max Steady State Velocity	Ra
1	0.01,0.01	2.77×10^{-4}	3.877×10^{-5}	2.7×10^{6}
2	1, 0.01	1.15×10^{-2}	1.23×10^{-3}	2.7×10^{8}
3	0.0001, 0.01	1.73×10^{-7}	2.71×10^{-8}	2.7×10^{4}

In case 1 of the 2-D transient models, the reduction in vertical acceleration from 1 to 0.01 g reduces the stability of the fluid against convection. As a result, this calculation shows

the fluid velocity increasing by three orders of magnitude. A comparison of the two steady state velocities ($v=8.9 \times 10^{-8}$ and case 1 3.8×10^{-5}) demonstrates this observation. Case 2 shows how high rates of convection result where a high lateral acceleration occurs while the vertical stability is decreased. The high flow skews the temperature isotherms or thermal profile in the liquid. The convective heat transfer rate is so high that it becomes greater than the conductive heat transfer rate. This is the explanation of the skewness of the temperature profile and of the high convection rate.

Case 3 shows another stable condition except that the g-levels are reduced from the pre-perturbation values. Note that the velocities of case 3 at steady state are higher than the pre-peturbation levels because the overall stability is lower. This confirmed a non-intuitive result at lower g-level may not result in lower convection. Do notice, however, that for these cases, and the above statement of lower g-level, that a low honzontal g-level is constantly impressed. What value it has cannot be experimentaly fixed, but it is clearly not zero. Comparing case 1 and 3 shows that if the horizontal g-level becomes proportionately higher, then convective flow can increase unless the vertical g-level is adjusted accordingly. Another consequence of this observation is that if an experiment is under 'low-g' conditions, minimum convection may not be established if other (lateral) accelerations are present. (An additional note is the consideration of rotational accelerations which have not been measured. Clearly, even during 'low-g', such rotational accelerations must impact the experiment to a similar degree as the lateral accelerations.)

The g-levels selected for use in the models have been observed on the KC-135. It should be emphasized that the duration of any low g-level like 0.0001 g is brief and cannot last a full 20 seconds as they do in the models. Consistent periods of low g-level have been achieved for several seconds. Also, these results are of 2-D models. To truly model the KC-135 environment, 3-D models with transient g-levels in three axes would be required. Three axis g-levels were not possible to model with Easyflow. 3-D models with two acceleration vectors were modeled as shown in the next section. (note: the result of the observations show that the modeling of flow should include 6 degrees of freedom where three are rotational accelerations. No one before has even considered such a model.)

The results from the 3-D models which were set up similarly to the 2-D models are similarly consistent. Due to the time to run the large models, the transient interval used was not 20 but rather 8 seconds. Again, the time cuts were made at one second intervals. Comparison of the results showed values were consistently matching between the two model types. For this, it is possible to develop confidence in the 2-D models and save the expense of performing many runs with the 3-D models. One value did not match between the two models and cases, and that was case 3 maximum velocity before steady state. In the 3-D model, the value closely matchs the velocity for steady state, while with the 2-D model, the maximum value overshoots considerably. There is no immediate explanation and other than this one value, the 2 and 3 dimensional models are comensurate with one another. Case 3 shows what happens where reducing gravity while maintaining a stable gravity level ratio between vertical and horizontal. The maximum

transient velocity occured at 1 second and had a value not much different from the steady state value. Within the resolution of this set, damping of the flow is clearly rapid.

3-D Transient Results Chart

For height=68 mm, width=15 mm and length=15 mm;
for top wall hot @ 50 °C, and bottom wall cold @ 25 °C;
with either walls adiabatic;
with water having Pr=6.7 and a=3.619 x 10^{-4} and k= 1 .494 x 10^{-3} cm/s
and V = 6.902E-3 cm^2/s; with $\Delta T=25°$ and starting conditions of steady state
1g in Y and 0.01g in X where U=2.78 x 10^{-9}, V=8.93 x 10^{-8} and W=2.76 x 10^{-8};
then:

CASE	Gravity	Max Velocity	Max Steady State Velocity	Ra
1	0.01,0.01	2.30 x 10^{-4}	4.13 x 10^{-5}	2.7 x10^6
2	1, 0.01	1.22 x 10^{-2}	1.47 x 10^{-3}	2.7 x10^8
3	0.0001, 0.01	1.91x10^{-7}	5.144 x 10^{-7}	2.7 x10^4

Figures 2 through 4 at the back of the report show a color representation of the three cases.

In order to evaluate another form of transient on the flow, two additional 2-D models were prepared where the steady state condition of 1 g vertical and 0.01 g horizontal is perturbed for one second with accelerations of 0.01 g vertical and 1 g honzontal and there allowed to settle to the settings in the chart below.

Due to the intensive, brief perturbation, the transient solutions at a specific point in the cavity of the cell oscillate sharply about the steady state solution. This observation comes from studying the raw, calculated data. Case 1 and case 4 still retain similar solutions at steady state. Also, as explained earlier, the steady state value for case 5 is lower than case 4 since the horizontal acceleration is 10 times less.

The model displays a maximum, convective velocity at one second after the perturbation. The value of the convective flow is not much different from the maximum horizontal velocity (V) after 1 second of high horizontal g. Such a large (1 g) horizontal transient is not likely to occur on the KC-135. What is interesting, is that after one second, the velocities diminish or are damped.

2-D Special Transient Results Chart

For height=68 mm, width=15 mm, aspect ratio=H/W=4.53;
for top wall hot @ 50 °C, and bottom wall cold @ 25 °C;

with side walls adiabaic; with water having Pr=6.7 and a = 3.619x 10^{-4} and k = 1 .494x 10^{-3} cm^2/s and V=6.902x 10^{-3} cm^2/s; with ΔT = 25 °C, U=1.717x 10^{-5} and V=6.218x 10^{-3} then:

CASE	Gravity	Max Velocity	Max Steady State Velocity	Ra
4	0.01,0.01	4.37 x 10^{-3}	3.56 x 10^{-5}	2.7 x 10^{6}
5	1, 0.01	5.21 x 10^{-3}	2.019 x 10^{-6}	2.7 x 10^{8}

3.4.2.3 Modelling the CFA Experimental Cell

To this point, models were developed which were ideal versions of the CFA experimental cell. The exact dimensions and thermal configuration were not detailed to the degree of the following models. For example, the earlier models were of an enclosed cavity where the top face was the only heat source and maintained at constant temperature. Similarly for the bottom face. Adiabatic walls were assumed for the side wall where in fact they were thin glass plates. In reality, due to design, the CFA cell had a heater which enclosed the upper quarter of the cell volume, which includes part of the side walls. The case was the same for the cold end with the cold brass block for cooling. Thus heat flow at the ends was not simply from a plane, but rather from a volume. The interior of the hot volume was free to convect as was the interior of the cold volume.

To further clarify, the actual dimensions are herewith given:

height of fluid volume = 115 mm,

width and depth of fluid volume = 15 mm

a 25 mm deep portion of the cell is inserted in a heated auminum block

a 25 mm deep portion of the opposite end of the cell is inserted in a cooled brass block

a 1 mm hole is in the end face of the fluid volume in the cold block to permit free expansion of heated fluid

for the model, the hot surfaces are 50 °C and the cold surfaces are 25 °C.

As before, with transient modeling, the steady state conditions were established with 1 g vertical (y) and 0.01 g honzontal (x). The initial velocities were U=2.07x 10^{-8}, V=5.28x 10^{-8} and W = -3.15x 10^{-8}. Clearly all velocities are very small and would be immeasurable in the CFA. Again also, the time range for the transient calculations was 8 seconds with the cuts made at 1 second intervals. To calculate Ra, the same values of a, k, and U as above were used.

CFA Model Results

CASE	State	Gravity	Max Velocity	Max Steady State Velocity	Ra
1	Steady	1		6.475×10^{-8}	1.3x109
2	Steady	0.01		6.436×10^{-9}	$1.3x10^{7}$
1	Transient	0.01,0.01	2.747×10^{-4}	3.64×10^{-5}	$1.3x10^{7}$
2	Transient	1, 0.01	1.436×10^{-2}	4.34×10^{-3}	$1.3x10^{3}$
3	Transient	0.0001, 0.01	1.908×10^{-7}	1.130×10^{-7}	$1.3x10^{5}$

These caculations were done as a check for the earlier ones and proved to have the same results in all respects. The maximum velocitis have the same order of magntide. The isotherms have the same patterns in the middle, uncovered part of the cavity. This repsesents the area one observes in the experiment.

The model showed small convective regions developing in the covered ends. This was due to the heat transfer requirement which was skewed due to the convection loop established between the ends of the cell. Cool liquid would flow into the hot volume and as it warmed, turn around and return to the cold end where the similar process would occur. This merely extended the heat transfer into surfaces into the heater and cooler interior walls.

3.4.2.4 Results from CFA Models

For the Raleigh number range of conditions used experimentally, which was 2.7×10^{4} to 2.7×10^{8}, the fluid flow pattern would be prodicted to be a single, simple circulating cell. Flow rates would be sufficiently low that laminar flow conditions would persist everywhere within the cuvette. The models all provided these similar results. Flow velocities for reasonably stable conditions of 0.01 g vertical and 0.01 g horizontal were predicted to be less than 4×10^{-5} m/s. This is for the conditions of a 1 x 1 x 5 cm cuvette volume filled with water and a temperature difference of 25 degrees. The models were selected based upon reasonable scenarios of acceleration levels and temperatures. Accelerations on the aircraft are far from constant but do achieve a steady state level. A review of acceleration patterns observed on the KC- 1 35 show that periods of time do exist where vertical gravity is a sustained 0.01, 0.001, and even occasionally 0.0001 gravity, at least for a few seconds.

Lateral accelerations can also range within these values with 0.01 and 0.001 being typical levels whether in high g or low g conditions. Occasions were found where the lateral g level exceeded the vertical during low g periods. The significance of this is that the fluid motion responds to all accelerations and non-zero lateral accelerations do cause fluid flow just as easily as vertical accelerations. Three simultaneous acceleration vectors were not supported by the Easyflow software. To seriously work with models with only vertical accelerations would be highly unrealistic (for the work performed here or in other convective experiments with very low velocities).

3.4.3 Comparisons Between Models and Experiments.

vertical accelerations would be highly unrealistic (for the work performed here or in other convective experiments with very low velocities).

3.4.3 Comparisons Between Models and Experiments.

3.4.3.1 Thermal Fluctuations Comparisons

The Easyflow models provided the ability to monitor temperature changes at a point within the cell during transient analysis.

3.4,3.2 Flow Motion Comparisons

All the models showed that flow streamlines developed into single circulation loops within the cell. The fluid velocity there, is the only real factor for comparison. For many conditions, the pure fluid velocity caculated was less than detectable by the CFA apparatus. The models do show where fluid velocities increase and often, during transients the velocities could be orders of magnitude greater than the limit of velocity resolution.

3.4.3.3 Non-thermal Gradient Study

One experient was flown which had no thermal gradient imposed on the specimen cell. Again, flake tracers were used to determine the flow patterns. What was observed makes comparisons between expeeriment and model simple. The only flow observed in the no-gradient case was during acceleration transients. Pitch over and rotational accelerations were the only sources of convection observed. There was no bouyancy driven or natural convective flow found because there was no temprature gradient. The significance of this is that the velocities calculated by the models for various conditions would be immeasurably small with a thermal gradient imposed. Faster flows were induced by other sources than those by thermal convection.

4.0 CONCLUSION

Convective flow experiments performed on the KC-135 indicate that convective flows are reduced substantially during the low gravity period of the parabolic flights. Observations of deleterious accelerations from plane motions are also observable. A means to quantitatively determine g levels from observations of fluid motion is not available at this time.

Free convective flow models have been developed using Easyflow software. These models correlate quite well with the observations in the KC-135 experiments. Our analysis indicates that correlation between this type of software and experimental data can provide useful information for the experimenters who are performing fluid experiments on the KC-135 and need to separate out high quality parabolas from those of lesser quality.

microgravity flow visualization system. Also we wish to thank Ms. Yan Chen for her hard work in performing the Easyflow simulations. Dr. William Kaukler was a primary contributor to the many ideas presented here and very important to the performance of this work. Also we wish to thank Dr. Gary Rosen from Clarkson University for his helpful suggestions on the lighting for the flow visualization.

5.0 BIBLIOGRAPHY / REFERENCES

1. G. Muller, "Convection in Melts and Crystal Growth", Adv. Space Res. 3, (1983) pp 51-60.

2. G. Muller, G. Neumann and W. Weber, "Natural Convection in Vertical Bndgman Configurations", Jour. Crystal Growth, 70 (1984) pp. 78-93.

3. Gregory T. Neugebauer and William R. Wilcox, "Convection in the Vertical Bridgman-Stockbarger Technique", Jour. Crystal Growth, 89 (1988) pp. 143- 154.

4. B-I Fu and S. Ostrach, "The Effects of Stabilizing Thermal Gradients on Natural Convection Flows in a Square Enclosure",

5. S.R. Coriell, R.F. Boisvert, J.I. Mickalonis, and M.E, Glicksman, "Morphological and Convective Instabilities during Solidification", Adv. Space Res. 3 (1983) pp 95 - 101.

6. P. R. Griffen and S. Motakef "Influence of Non Steady Gravity on Natural Convection During Microgravity Solidification of Semiconductors - Part 1. Time Scale Analysis", Appl. Microgravity Tech. II (1989) pp121 - 127.

7. P. R. Griffenn and S. Motakef "Influence of Non Steady Gravity on Natural Convection During Microgravity Solidification of Semiconductors - Part 2. Implications for Crystal Growth Experiments", Appl. Microgravity Tech. II (1989) pp 128 - 132.

8. V. S. Avduyevsky, et al, "Scientific Foundations of Space Manufacturing", Published by Mir Publishers, Moscow, 1984.

9. L. W. Sparedley, S. V. Bourgeois, and F. N. Lin, "Space Processing Convection Evaluation: G-Jitter Convection of Confined Fluid in Low Gravity", AIARE 10th Thermophysics Conferance, Denver, CO 1975, paper 75-695

10. Y. Kamotani, A. Prasad, and S. Ostrach, "Thermal Convection in an Enclosure Due to Vibrations Aboard Spacecraft", AIARE Journal 19, (1981) pp 511 - 516

APPENDIX

Figure 1. The Convective Flow Analyzer Experiment Package and Data Acquisition Rack.

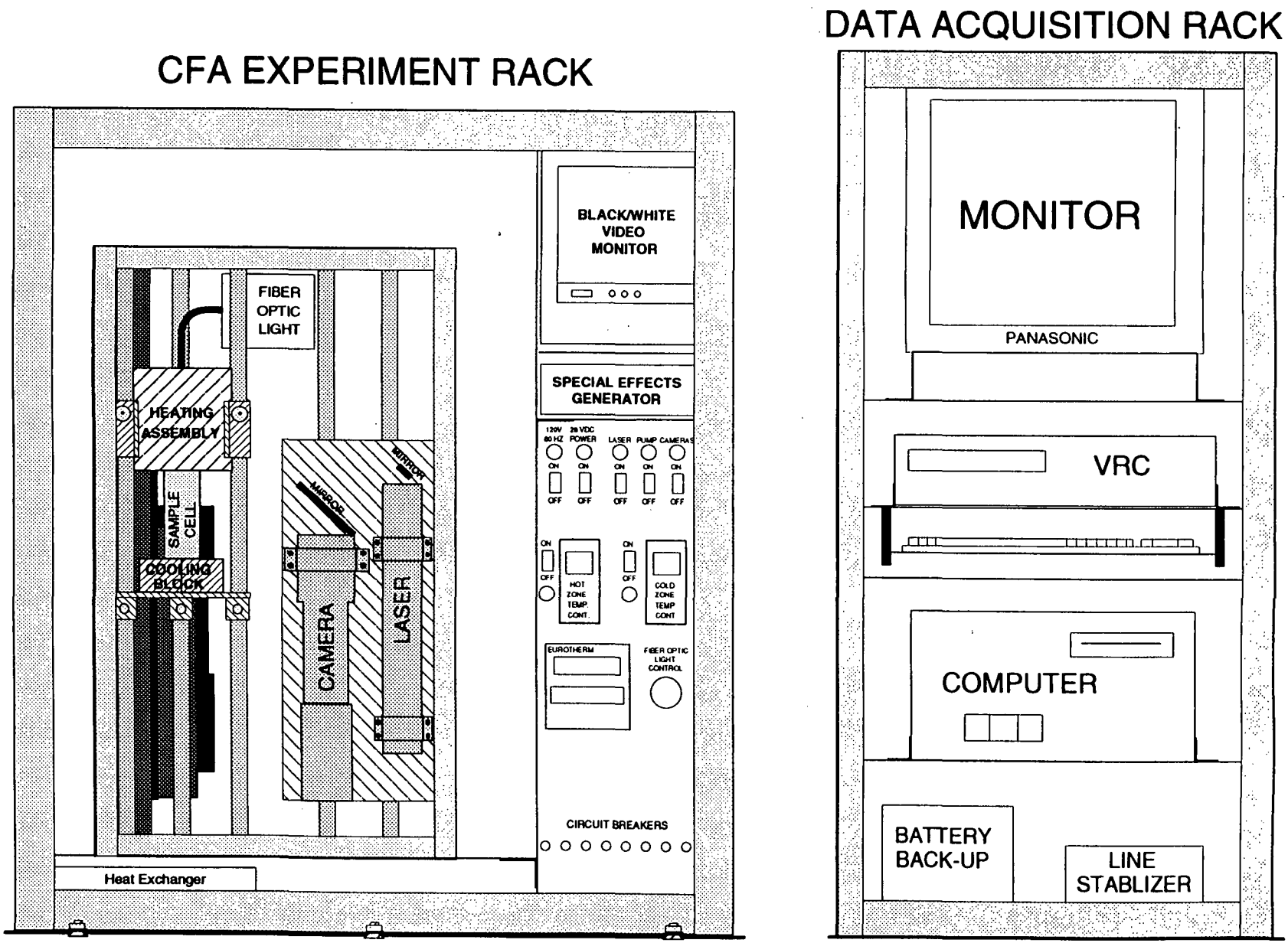

APPENDIX

Magnification and Resolution calculation for CFA cameras

Camera model Javelin JE2362A
high resolution 2/3 inch MOS
340 lines horizontal res
576 x 485 pixels
representing 8.8 x 6.6 mm scan
min illum. 3 lux with f1.4 lens

sensor diagonal: $sd := 11$ mm

sen vert: $sv := 6.6$ mm

sen horiz: $sh := 8.8$ mm

horiz pix: $hppmm := \frac{576}{sh}$ $hppmm = 65.455$

horiz pix size: $hps := \frac{sh}{576}$ $hps = 0.015$ mm

$vps := \frac{sv}{485}$ $vps = 0.014$ mm

cuvette width: $cw := 14$ mm

4.4 mm of sensor represents 14 mm of cuvette width
which is 576/2 pixels wide

$$pix2 := \frac{576}{2} \qquad pix2 = 288$$

14 mm of cuvette will be divided into 288 pix horiz.

$$res := \frac{cw}{pix2} \qquad res = 0.049 \text{ mm}$$

monitor height is 5.25 and width is 7 inches

ratio half monitor height to width is 5.25/3.5
to give vertical
field of view on 14 mm cuvette

$$rat := \frac{5.25}{3.5}$$

$$rat = 1.5$$

height in mm of cuvette is..

$vhtc := 1.5 \cdot 14$ mm

$vhtc = 21$

vertical resolution is 21 mm by 485 pix

$resv := \frac{vhtc}{485}$ $resv = 0.043$ mm

Resolution of points is maximum of 49 x 43 microns hor x vert at the cuvette in the plane of focus. This means that if two particles are closer than 50 microns together, and are smaller than 50 microns in size, they will be seen as if they are one.

Calculation of Settling rate of Latex Spheres in water and of Guanine Flakes in water or perchloroethylene

---

CONSTANTS and UNITS

$L \equiv 1$ $T \equiv 1$ $M \equiv 1$ $cm := 1L$ $gm := 1M$ $sec := 1T$

$m := 100 \cdot cm$

$deg \equiv 1$ $kgm := 1000 \cdot gm$

gravity $g := 9.8 \cdot \frac{m}{sec^2}$

visc η is dyne-sec/cm^2 or poise

$poise := 1 \cdot \frac{gm}{cm \cdot sec}$ $cp := \frac{poise}{100}$

$dyne := 1 \cdot gm \cdot \frac{cm}{sec^2}$

a stoke is kinematic viscosity

$erg := 1 \cdot dyne \cdot cm$ $\rho_\lambda := 1$

$stoke := \frac{poise}{\rho_\lambda}$

$joule := 10^7 \cdot erg$ $kJ := 1000 \cdot joule$

$watt := \frac{joule}{sec}$ $mW := \frac{watt}{1000}$ $hr := 3600 \cdot sec$

---

density of styrene sphere

$\rho_\sigma := 1.05 \cdot \frac{gm}{cm^3}$

density of water average value...

$\rho_\lambda := 1 \cdot \frac{gm}{cm^3}$

Stoke's Law ... written two ways.....

$\lambda := 1 \cdot \frac{cm}{sec}$ arbitrary fixed velocity of shere

$r := 30 \cdot 10^{-6} \cdot m$ radius of sphere

$\eta := 1 \cdot poise$ arbitrary fixed viscosity

$f := 6 \cdot \pi \cdot \eta \cdot r \cdot \lambda$ Stoke's Law says f is force on sphere moving with velocity λ@ through liquid of viscosity η

$\lambda := 2 \cdot g \cdot r^2 \cdot \frac{\rho_\sigma - \rho_\lambda}{9 \cdot \eta}$

$f = 0.057 \cdot gm \cdot cm \cdot sec^{-2}$

Stoke's law for a sphere falling through a liquid under the influence of gravity

$\lambda = 9.8 \cdot 10^{-5} \cdot cm \cdot sec^{-1}$

from CRC...

for 20 to 100 C, viscosity is calculated...

$i := 0..100$

$T_i := i$ $\eta_{20} := 1.002 \cdot cp$

$$RHS_i := \frac{1.3272 \cdot [20 - T_i] - 0.001053 \cdot [T_i - 20]^2}{T_i + 105}$$

$$\eta_i := \eta_{20} \cdot \left[10^{RHS_i}\right]$$

$\eta_{50} = 0.547 \cdot cp$

$\eta_{100} = 0.282 \cdot cp$

$\eta_0 = 1.777 \cdot cp$

although not accurate the fit works to zero degrees C rather well

from CRC...

for 0 to 100, the density of air-free water is a table

$\rho_i := 0 \cdot \frac{gm}{cm^3}$

$\rho_0 := .99987 \cdot \frac{gm}{cm^3}$ $\rho_5 := .9999999 \cdot \frac{gm}{cm^3}$ $\rho_{10} := .99973 \cdot \frac{gm}{cm^3}$

$\rho_{20} := .99823 \cdot \frac{gm}{cm^3}$ $\rho_{30} := .99576 \cdot \frac{gm}{cm^3}$ $\rho_{40} := .99224 \cdot \frac{gm}{cm^3}$

$\rho_{50} := .98807 \cdot \frac{gm}{cm^3}$ $\rho_{60} := .98324 \cdot \frac{gm}{cm^3}$ $\rho_{70} := .97781 \cdot \frac{gm}{cm^3}$

$\rho_{80} := .97183 \cdot \frac{gm}{cm^3}$ $\rho_{90} := .96534 \cdot \frac{gm}{cm^3}$ $\rho_{100} := .95838 \cdot \frac{gm}{cm^3}$

$j := 0, 10..100$

Plot data only every 10 degree interval, j, next page...

Density of water as function of temperature

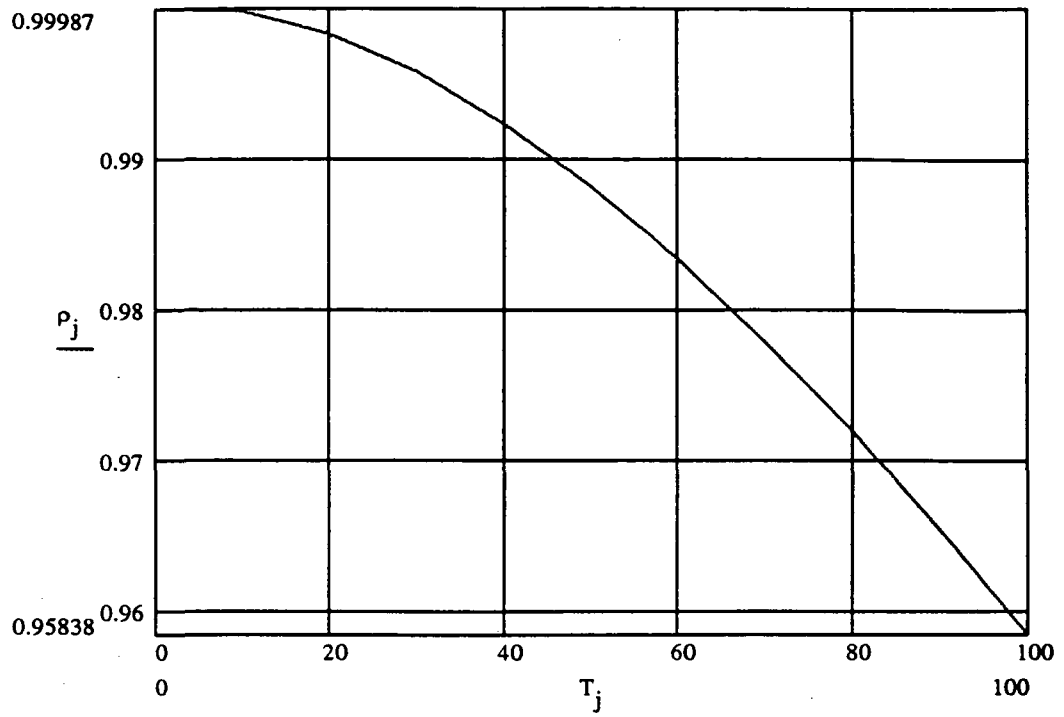

Viscosity of water as a function of temperature in poise

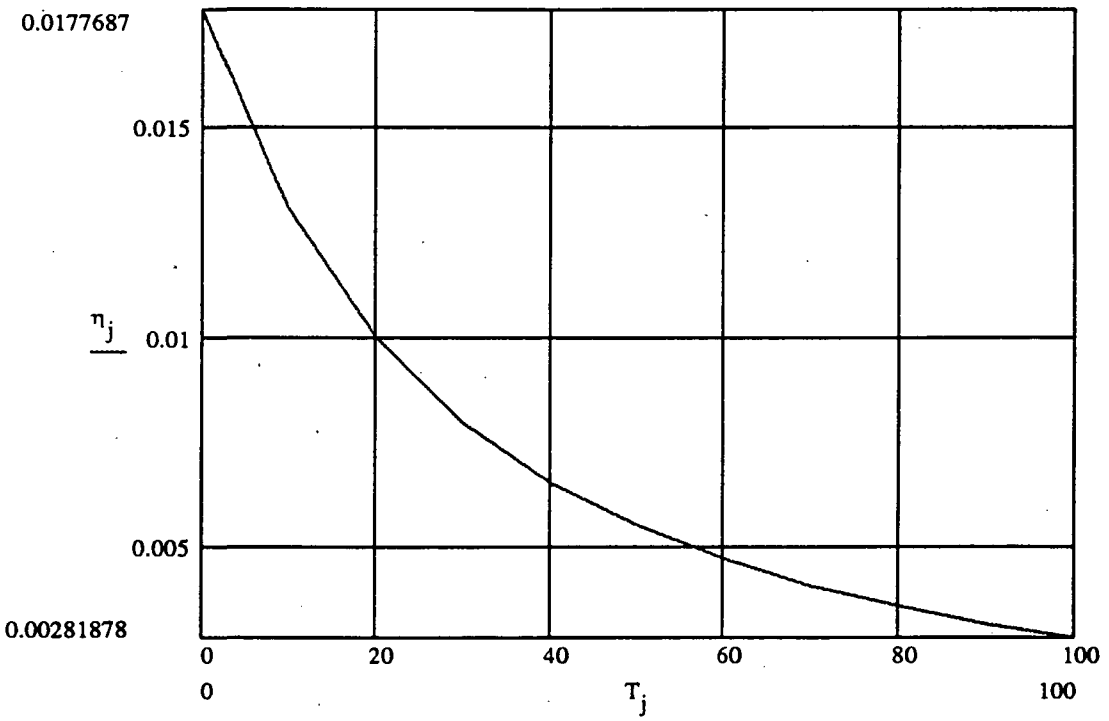

$$v_i := 2 \cdot g \cdot r^2 \cdot \frac{\rho_\sigma - \rho_i}{9 \cdot \eta_i} \qquad r_2 := 10 \cdot 10^{-6} \cdot m \qquad v2_i := 2 \cdot g \cdot r_2^2 \cdot \frac{\rho_\sigma - \rho_i}{9 \cdot \eta_i}$$

Stoke's velocity for
latex sphere in water
as a function of temperature
assuming styrene stays constant
density with temperature

Stokes settling velocity in cm/sec
as a function of temperature deg. C
for styrene spheres in water

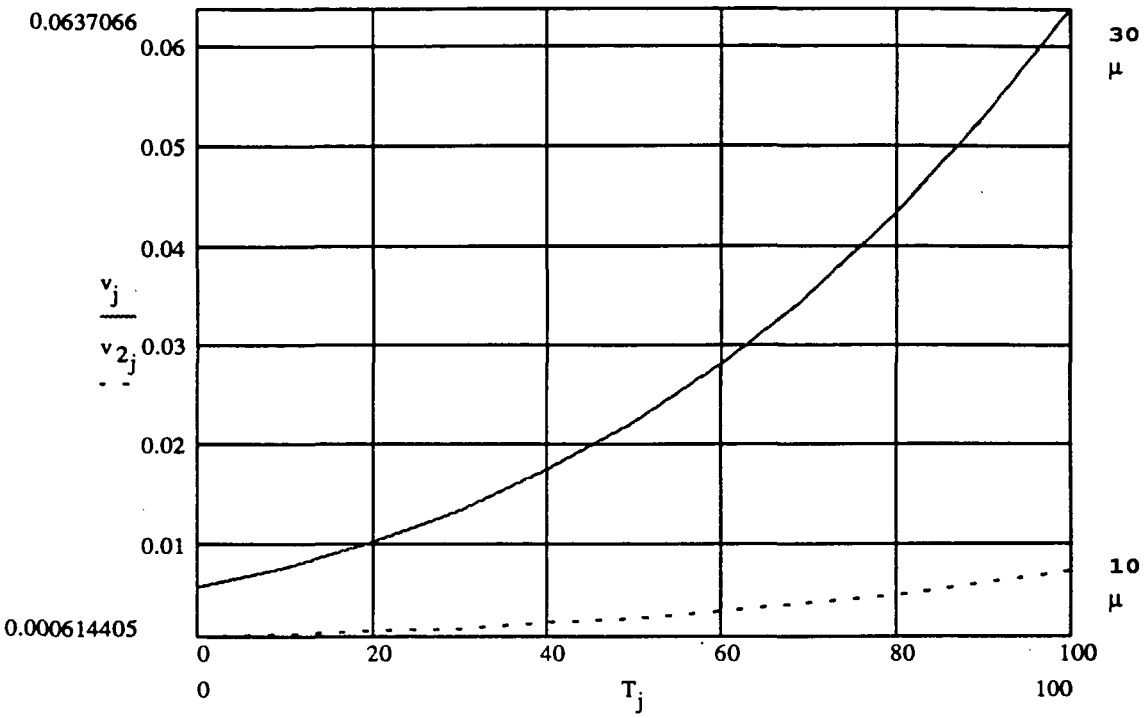

Stokes calculations for Guanine Flakes in water and
perchloroethylene
and carbon tetrachloride

$\rho_{\pi\chi} := 1.620 \cdot \frac{gm}{cm^3}$

$\rho_{\chi\tau} := 1.593 \cdot \frac{gm}{cm^3}$

densities of
perchloroethylene and
carbon tetrachloride
at 25 deg. C, room
temperature

$\rho_{\phi} := 1.62 \cdot \frac{gm}{cm^3}$

density of Guanine
Flakes

flakes have dimensions of 6 x 30 x 0.07 micrometers
and have a settling rate in water of 0.1 cm/hr
their refractive index is 1.85
this is based on paper: P. Matisse and M. Gorman in
The Physics of Fluids, v27, n4 Apr. 1984, p. 759

The flakes are supposed to be best used for flow visualization in low Prandtl number fluids.

$v_f := 0.1 \cdot \frac{cm}{hr}$ $\quad v_f = 2.778 \cdot 10^{-5} \cdot \frac{cm}{sec}$ settling velocity in water at room temperature

$r_f := \sqrt{\left[2 \cdot g \cdot \left[v_f^{-1}\right] \cdot \frac{\rho_\phi - \rho_{20}}{9 \cdot \eta_{20}}\right]^{-1}}$ $\quad \rho_{20} = 0.998 \cdot mass \cdot length^{-3}$

$r_f = 4.534 \cdot 10^{-7} \cdot m$ $\quad \eta_{20} = 0.01 \cdot mass \cdot length^{-1} \cdot time^{-1}$

according to these calculations, a flake appears to have an effective radius of 0.45 micrometers in water

---

Prandtl number calculations for water

$c_p := 4.184 \cdot \frac{\frac{kJ}{kgm}}{deg}$ specific heat at constant pressure

$\mu := 1 \cdot poise$ dynamic viscosity or absolute viscosity called η above.....maybe

$k := 5.98 \cdot \frac{\frac{mW}{cm}}{deg}$ thermal conductivity coefficient here at 290 K

$\rho_{\rho\varepsilon\phi} := \rho_\lambda$

$D := \frac{k}{c_p \cdot \rho_{\rho\varepsilon\phi}}$ thermal diffusivity

η is supposed to be kinematic viscosity in poise

$Pr := c_p \cdot \frac{\mu}{k}$

$Pr = 699.666$

FOLDOUT FRAME 1

FOLDOUT FRAME 2

EASY FLOW MODELS OF CONVECTIVE AND TEMPERATURE FLOWS IN REDUCED GRAVITY

Figure 2. Simulation showing effect of reducing gravity from 1 g to a stable 0.01g value for up to 18 seconds in a Bridgman furnace configuration with the heat source at the top. Total temperature drop across the sample is 25° C.

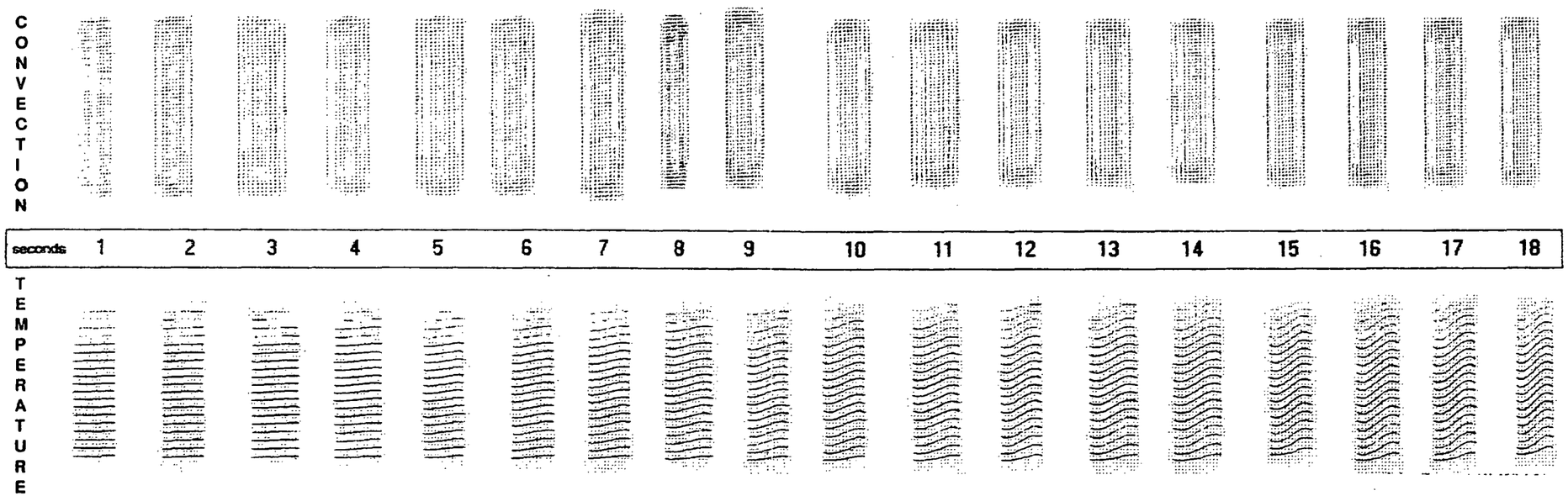

STREAMLINES ARE SCALED FROM 3 x 10^{-3} m/

FOLDOUT FRAME 1.

FOLDOUT FRAME 2.

EASY FLOW MODELS OF CONVECTIVE AND TEMPERATURE FLOWS IN REDUCED GRAVITY

Figure 3. Simulation showing effect of reducing gravity from 1 g to 0.01g. A perturbing force is simulated by a transient horizontal g of 1 which then drops to a stable 0.01 g value for up to 18 seconds.

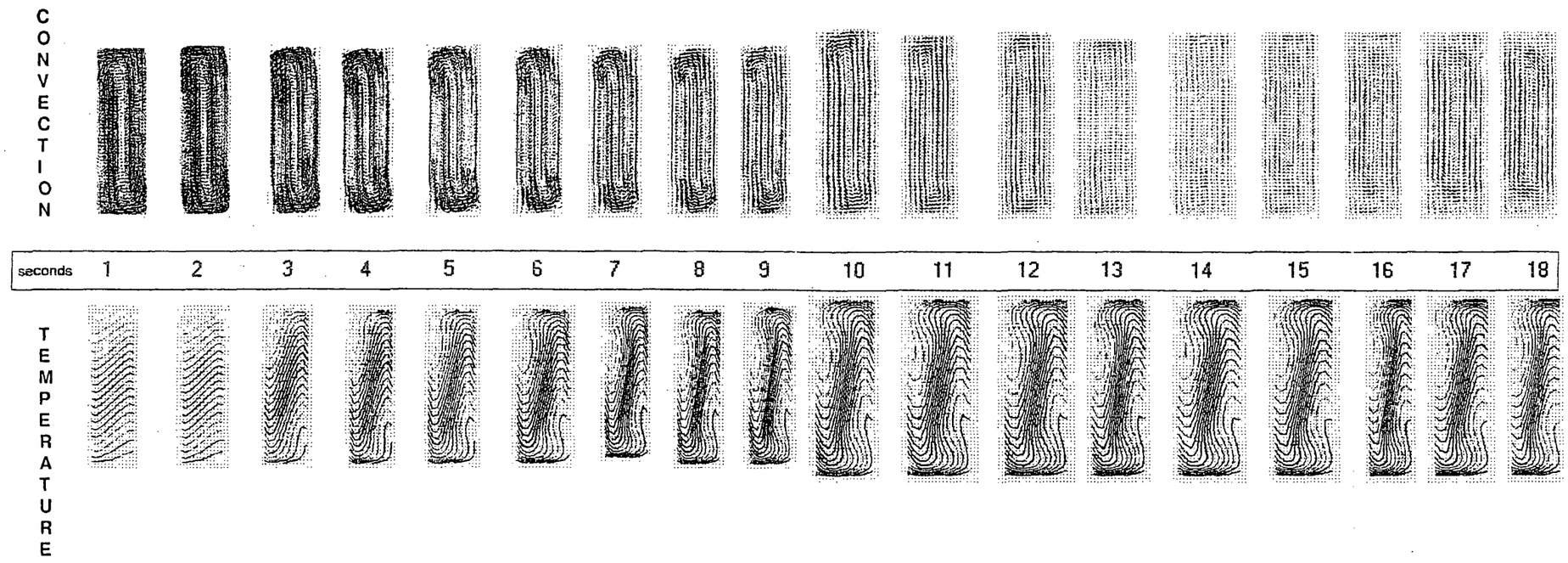

STREAMLINES ARE SCALED FROM 3 x 10^{-3} m/s

FOLDOUT FRAME 1.

FOLDOUT FRAME 2.

EASY FLOW MODELS OF CONVECTIVE AND TEMPERATURE FLOWS IN REDUCED GRAVITY

Figure 4. nulation showing effect of reducing gravity from 1 g to 0.001g. A perturbing force is simulated by a transient horizontal g of 1 which then drops to a stable 0.001 g value for up to 18 seconds.

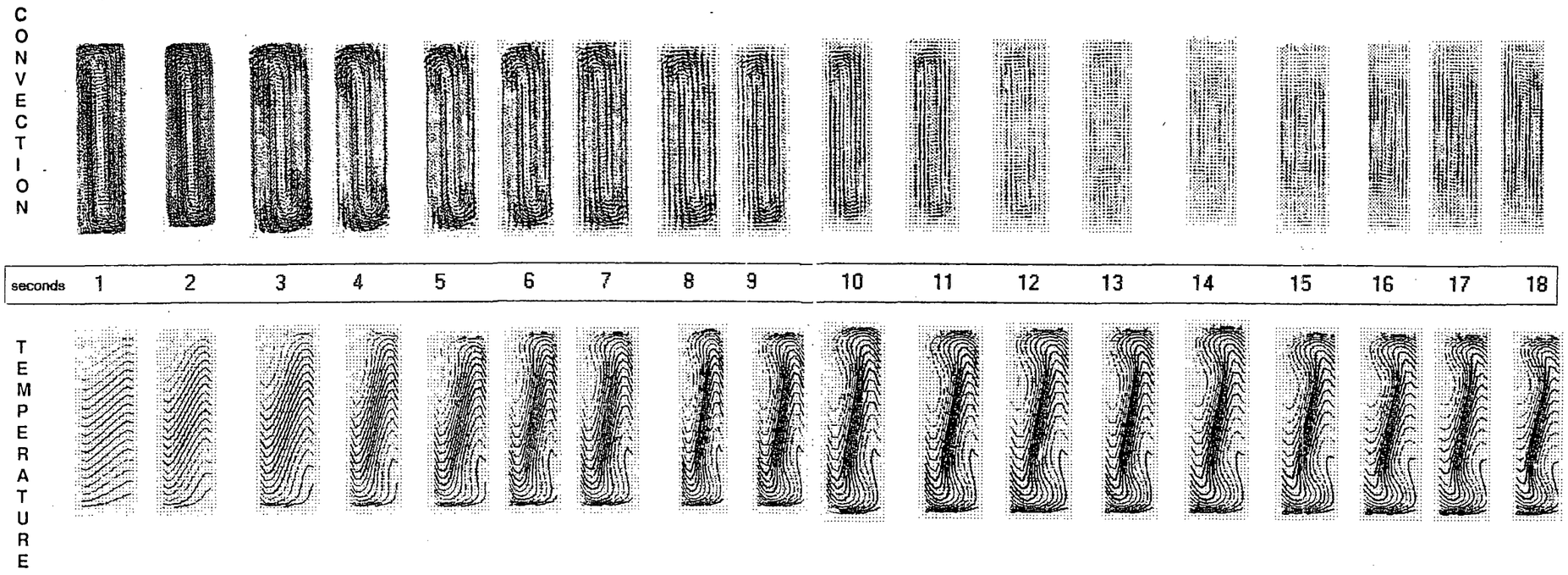

STREAMLINES ARE SCALED FROM 3 x 10^{-3} m/s